

## BOREHOLE CEMENT SHEATH INTEGRITY - NUMERICAL SIMULATION UNDER RESERVOIR CONDITIONS.

Ricardo M. Ramos<sup>a,b</sup> and Ariel Sánchez Camus<sup>c,d</sup>

<sup>a</sup>*Solaer Ingeniería, Solaer Ingeniería Argentina SA, Calle 31 No 1905, 1900 La Plata, Argentina,  
rmos@solaeingenieria.com, <http://www.solaeingenieria.com>*

<sup>b</sup>*Facultad de Ingeniería, Universidad Nacional de La Plata, Calle 1 y 47, 1900 La Plata, Argentina*

<sup>c</sup>*Solaer Ingeniería, Solaer Ingeniería Argentina SA, Calle 31 No 1905, 1900 La Plata, Argentina,  
acamus@solaeingenieria.com, <http://www.solaeingenieria.com>*

<sup>d</sup>*Depto. de Geofísica Aplicada, Universidad Nacional de La Plata, Paseo del Bosque s/No, 1900 La  
Plata, Argentina*

**Keywords:** cement sheath, zonal isolation, reservoir conditions, numerical simulation.

**Abstract.** The most important function of the cement sheath is to provide zonal isolation in a production well. To achieve this objective, a hydraulic seal must be obtained between the casing and the cement, and between the cement and the formation. Throughout the life of a production well the cement sheath is subject to different reservoir conditions. Drilling, changes in pressure and temperature due to production, stimulation, and natural tectonic activity can lead to cement damage. Smaller chronic leakages due to defective well tubulars or damaged cement sheaths in the well cause a loss in the sustained casing pressure (SCP). Ensuring well integrity means to protect the environment against leakage along the well and to guarantee its producing potential. The tool presented in the current paper allows the cement engineer to simulate underground well conditions. After simulating the chosen scenario, various outputs can be combined in the overall analysis, including compression, traction, thermo-elasticity, and microannulus to help the cement engineer to analyze and design the proper cement to be used during the completion process.

## 1 INTRODUCTION

The disappearance of cement bond log response as a result of the loss of proper zonal isolation has been observed in numerous wells, even in those where the cement was properly placed providing an initially good hydraulic seal, see [Thiercelin et al. \(1998\)](#). Since well construction materials are prone to degradation with age and upon exposure to downhole fluids, pressures and temperature variations, the number of well integrity problems tends to increase as the wells age. According to [Lavrov and Torsæter \(2016\)](#), a study of 15.500 wells in the Gulf of Mexico showed that as a well becomes 15 years old, it has a 50% probability of being affected by SCP. The overall percentage of wells suffering from this problem was about 35% in the Gulf of Mexico, and similar numbers have been reported for the North Sea. Without complete zonal isolation in the wellbore, the well may never reach its full producing potential. Remedial work required to repair a faulty cementing job may do irreparable harm to the producing formation. In addition to the possibility of lost reserves and lower producing rates, start-up of production (revenue) is delayed. Other problems may arise, such as not being able to confine stimulation treatments to the producing zone, or confining secondary and tertiary fields to the pay zone. Most of the problems related to loss of cement integrity can be traced back to improper cement placement, but adhesion and prevention of fracturing are also believed to be crucial for ensuring well integrity, see [Nelson and Guillot \(2006\)](#). The tool presented in this paper has the purpose of helping the cement engineer to simulate underground well conditions to guarantee well integrity. Simulating the borehole cementing process under reservoir conditions allows engineers to test different mechanical cement parameters to ensure zonal isolation and select the most economical alternative for the producing area. For a realistic analysis of the subsurface environment the chosen scenario can deal with anisotropic rocks (e.g shales, fractured sandstone, etc), anisotropic stresses, creep laws, thermo-elasticity effects, and poral pressure.

## 2 BOREHOLE CEMENT SHEATH INTEGRITY

Primary cementing is the process of placing cement in the annulus between the casing and the formations exposed to the wellbore. The most important function of the cement sheath is to provide zonal isolation in the wellbore e.g., to exclude fluids such as water or gas in one zone from oil in another zone. To achieve this objective, a hydraulic seal must be obtained between the casing and the cement, and between the cement and the formations, see figure (1). Annular seals are not always perfect and leakage along the well can occur. For a producing well, flow of fluids along the cement sheath is manifested either by the loss of reservoir fluids through cross-flow along the cement sheath, or by the influx of underground fluids from other formations into the active layer, see [Nelson and Guillot \(2006\)](#); [Lavrov and Torsæter \(2016\)](#).

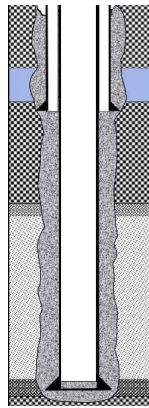
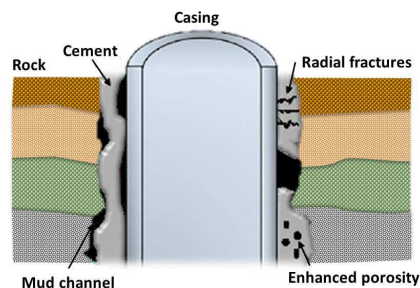


Figure 1: Borehole Cement Sheath.

Most Statal Departments of Environmental Protection around the world have strict policies regulating cementing practices in order to reduce the risk of inter-zonal communication and sustained casing pressure (SCP) due to substandard annular cement sheath integrity. SCP is caused by hydrocarbon fluid migration, mainly gas from the formation to the surface through communication pathways in the annulus, see figure (2). Depending on the degree of communication, the pressure build-up rate varies from well to well, and is usually bled off when the wellhead pressure rises to unsafe levels, see [Williams et al. \(2011\)](#); [Lavrov and Torsæter \(2016\)](#).

Figure 2: Leakage paths that can be present in a well-Modified from [Lavrov and Torsæter \(2016\)](#).

Drilling, changes in pressure and temperature (heating/cooling cycles) due to production, hydraulic stimulation, earth vibrations, formation fluid influx, and natural tectonic activity induce changes in the stress field that can potentially affect the cement sheath. The creation of an annulus is the consequence of fracture propagation within the cement sheath and/or the dislodging of the cement sheath from the casing or formation by overcoming the cement-to-casing and the cement-to-formation bond (figure (3)). As stated by [Nelson and Guillot \(2006\)](#); [Lavrov and Torsæter \(2016\)](#), all of these phenomena have to be taken into account when casing-cement sheath-formation system is performed.

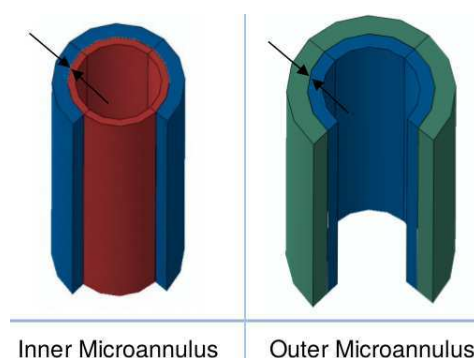


Figure 3: Casing/Cement microannulus-Cement/Formation microannulus.

One of the most detrimental events throughout the life of a production well is hydraulic stimulation. The pressure-induced causes casing expansion and therefore compression and tensile stresses on the cement sheath (figure (4)), may lead to cracking and compromising zonal isolation.

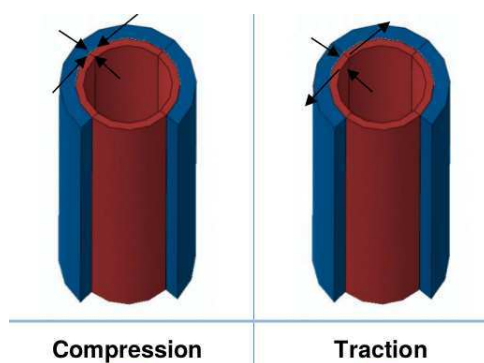


Figure 4: Compression and Traction efforts.

### 3 THEORETICAL ASPECTS

In this section a brief theoretical description of the constitutive-laws, physics equations, cement properties, and geological scenario to be used in the numerical model is presented. For further details, we recommend the following bibliography: [Lavrov and Torsæter \(2016\)](#), [Fjaer et al. \(2008\)](#) and [Zoback \(2007\)](#).

#### 3.1 Generalized Hooke's Law

Deformations in materials are termed strain and internal forces between different parts of the medium are called stress. Stress and strain do not exist independently; they are linked through the constitutive relationships that describe the nature of the material. Hooke's constitutive-law defines the most general expression for an elastic solid, and is a linear relation among all the components of the stress and strain tensor for small deformations.

$$\sigma_{ij} = c_{ijkl}\varepsilon_{kl} \quad (i, j, k, l = 1, 2, 3) \quad (1)$$

The stress tensor is denoted by  $\sigma_{ij}$ , the strain tensor by  $\varepsilon_{kl}$  and  $c_{ijkl}$  are the components of the material's fourth-order stiffness tensor. The fourth-order stiffness tensor has 81 components

with 21 of them being independent. These 21 components are necessary to specify the stress-strain relationship for the most general form of elastic solid. Equation (1) assumes perfect elasticity; there is no energy loss or attenuation as the material deforms in response to the applied stress.

### 3.2 Mohr-Coulomb's failure criterion in three dimensions

The stresses in the underground formations and around wells are generally anisotropic ( $\sigma_1 \neq \sigma_2 \neq \sigma_3$ ). Experimental evidence has shown that the intermediate principal stress ( $\sigma_2$ ) under shear conditions has a significant impact on the strength of several rock types, although minor compared to the effect of the other stresses. The Mohr-Coulomb complete failure surface is indicated in figure (5). The cross-section of the Mohr-Coulomb failure surface in a  $\Pi$ -plane is an irregular hexagon with sharp corners and threefold symmetry. The rock fails when the stress exceeds the failure surface, while it remains intact as long as the stress is lower than this limit surface.

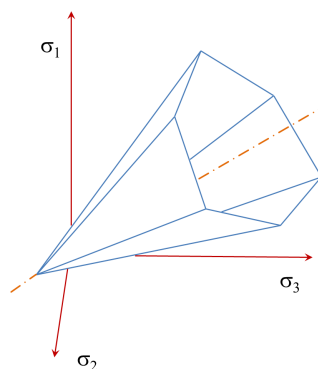


Figure 5: Mohr-Coulomb failure surface.

The effective stresses represent the forces transmitted through the rock skeleton. As the pore pressure is equal in all directions, it will affect only the normal stresses. Hence, increasing pore pressure may destabilize a rock with respect to shear and tensile failure. The concept of effective stress in terms of the Biot constant  $\alpha$  is based on the assumption that the rock is linearly elastic, and is not directly applicable for a rock at failure. However, it is generally accepted that Terzaghi's definition (2) of effective stress is the most relevant definition to be used in failure criteria, see Fjaer et al. (2008); Zoback (2007).

$$\sigma_i = \sigma_{ij}\delta_{ij} - \alpha p_f \quad (i, j = 1, 2, 3) \quad (2)$$

where  $\sigma_{ij}$  is the stress tensor,  $\delta_{ij}$  is the Kronecker delta function, and  $p_f$  is the pore pressure.

### 3.3 Plasticity

Plasticity is a concept describing non-elastic deformation of a material. Plastic deformation is not recovered when the load causing the deformation is released. The theory of plasticity is designed to model ductile behavior, that is, behavior in which the material can sustain a load comparable to the failure load well beyond failure. The theory of plasticity is based on four major concepts:

1. Plastic strain. The total strain increment associated with a stress increment is assumed to consist of an elastic part and a plastic part:

$$\varepsilon_{ij} = \varepsilon_{ij}^e + \varepsilon_{ij}^p \quad (i, j = 1, 2, 3) \quad (3)$$

$\varepsilon_{ij}^e$  is related to the stress increment by conventional elasticity theory, and will vanish when the stress is released. The plastic strain  $\varepsilon_{ij}^p$  is a permanent deformation, and will remain when the stress is relieved.

2. A yield criterion. The yield point is the point at which irreversible changes occur in the material. Hence, the yield point represents the onset of plastic deformation. A yield criterion is similar to the failure criteria defined and it defines the surface in stress space where plasticity is initiated.
3. A flow rule. The flow rule describes how the plastic strains develop for a given loading situation.
4. A hardening rule. A material under certain conditions may sustain increasing load after the initial failure. This is described by the hardening rule. The hardening may be interpreted as a change of the yield surface in principal stress space .

An ideally plastic material is a material that can endure infinite plastic strain without change in the stress level. After the initial elastic phase, the material deforms at constant stress.

### 3.4 Creep

Creep is a time-dependent deformation that may occur in materials under constant stress. Creep originates from visco-elastic effects in the solid framework. There are three stages of creep following a change in the stress state. The first stage, called primary (I) or transient creep is the region where the rate of the time-dependent deformation decreases with time. If the applied stress is reduced to zero during the primary creep stage, the deformation will eventually decrease to zero. In the second stage (II), known as steady state creep or secondary the deformation rate is constant. If the applied stress is reduced to zero during this stage, the deformation will not vanish completely. Steady state creep thus implies a permanent deformation of the material. The last stage, called accelerating or tertiary (III) creep, in which the deformation rate may increase with time. This stage leads rapidly to failure. Figure (6), shows the three stages described.

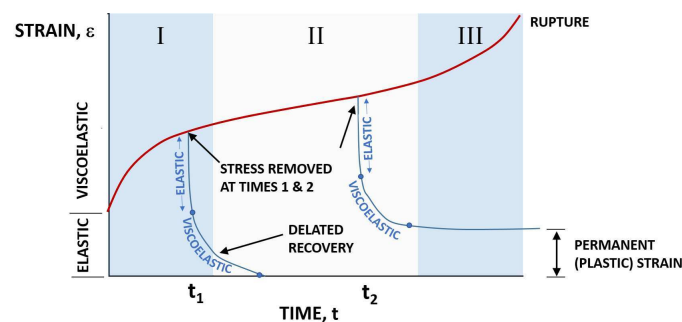


Figure 6: Creep Stages

The actual creep behavior of a material depends on the magnitude of the applied stress. For low or moderate stresses, the material may stabilize after a period of primary creep. For high stresses, the material may rapidly run through all three stages of creep and finally fail. Creep is a molecular process, and the time scale depends on temperature; the process generally speeds up with increasing temperature, see [Fjaer et al. \(2008\)](#).

### 3.5 Thermo-elasticity

The casing, cement, and rock formation are all considered to be thermo-elastic materials. Thermo-elasticity provides a linear relationship among the primary strains, stresses, and temperature. The total thermal expansion field is defined as:

$$\varepsilon^{th} = \tau(T, f_{\beta})(T - T^r) - \tau(T^0 - f_{\beta}^0)(T^0 - T^r) \quad (4)$$

$\tau$  is thermal expansion coefficient at the reference temperature  $T^r$ ,  $T$  is the current temperature,  $T^0$  is the initial temperature,  $f_{\beta}$  is the current values of the predefined field variables,  $f_{\beta}^0$  is the initial values of the field variables.

### 3.6 Stress tensor in the earth's crust

The underground stress state consists of the three mutually orthogonal principal stresses, plus the pore pressure. In the oil and gas industry, it is very common to assume that the vertical stress is a principal stress. Thus, one principal stress is generally normal to the earth's surface with the other two principal stresses acting in an approximately horizontal plane. This assumption is valid only at large depth within a homogeneous Earth, in areas which have not been exposed to tectonic activity or which are no remnant stresses from previous tectonic activity. The vertical stress is governed by gravity, which has a unique direction, pointing towards the centre of the Earth. Surface topography (stress free), heterogeneities such as inclusions, facies changes or faults cause lateral mass variations. Also, near underground openings such as boreholes, or near depleting reservoirs have significant influence on the direction of the stress field. The described phenomena cause that principal stress directions will differ from the vertical-horizontal orientation, see [Hofmann and Moritz \(2005\)](#); [Fjaer et al. \(2008\)](#); [Zoback \(2007\)](#). Instead of the above mentioned, it is generally reasonable and convenient to assume that the vertical is a principal stress direction, and the concept can even be applied up to the depth of the brittle-ductile transition in the upper crust at about 15-20 km depth as shown in figure (7).

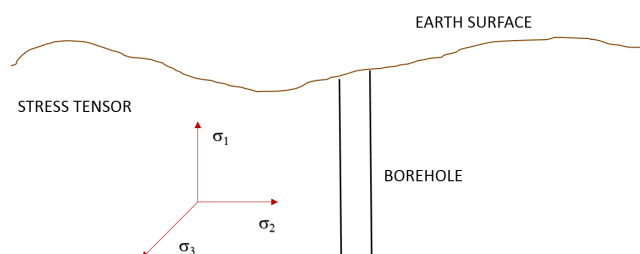


Figure 7: Crustal Stress Tensor.

### 3.7 Cement properties

The cement used in the oilwells is not the same as concrete used in civil engineering for construction. Concrete is a mixture of cement and aggregate particles (mainly sand), while cement

is a pure low-permeability binding material. A cement slurry is a mixture of cement and water in such proportion that solidification can occur. The solidification starts with setting, which is a rapid stiffening without significant strength development, followed by the slower hardening process which builds compressive strength. During a cementing job, cement undergoes a transformation from a liquid slurry being pumped down the wellbore to a solid material filling up the annular space between the casing and the borehole. While in the slurry state, the cement is characterized by rheological properties such as yield stress and plastic viscosity. The transition of cement from the liquid to the solid state is characterized by various properties such as volumetric change, rate of strength build-up or how easily formation fluids can enter the not-yet-solid cement. When hardened, cement is characterized by properties that determine how stable and permeable it is, how well it binds to the casing and the rock or how prone it is to fracturing. See [Lavrov and Torsæter \(2016\)](#).

### 3.8 Properties of the cement slurry

From a rheological point of view, cement slurries are non-Newtonian fluids. They have a yield stress, which means that a shear stress in excess of a certain threshold value must be applied in order to put the slurry into motion. When the shear stress in the slurry is above the yield stress, the slurry behaves as a viscous fluid. The existence of yield stress has significant implications for fluid flow in pipes and annuli. In particular, the shear stress is lower than the yield stress around the axis of the pipe. As a result, a hard core moving as a solid plug rather than a liquid develops around the axis of the pipe. The fluid thus flows as a liquid near the walls, where the shear stress is above the yield stress, and moves as a solid plug near the axis. See [Lavrov and Torsæter \(2016\)](#).

### 3.9 From slurry to solid cement

The hardening is due to hydration of cement which starts immediately or some time after the cement slurry has been mixed. Hydration involves changes in both the structure and the properties of cement. In the absence of an extra water supply, this causes neat cement to shrink. As a result of chemical shrinkage due to hydration, porosity and pore pressure decrease as setting proceeds. In addition to the decline in porosity and pore pressure, shrinkage may cause fracture growth in cement, see [Lavrov and Torsæter \(2016\)](#). Cement hydration is an exothermic reaction, i.e. heat is released as hydration proceeds. The heat released makes the temperature of cement increase during setting. This causes the casing diameter to be slightly larger than it otherwise would be during cement setting. When the temperature falls back to its regular value, a microannulus can be formed between the cement and the casing. The heat release during hydration also has a detrimental effect when cementing permafrost intervals as it may cause melting of the formation. This may lead to poor bonding and induce subsidence in the near-well region. During cement hydration, decreasing porosity results in a significant reduction of permeability, see [Backe et al. \(1997\)](#). The permeability of a cement slurry is on the order of 1D, while the permeability of hardened cement is on the order of 1 to 10  $\mu$ D. A model performed in civil engineering on concrete is presented just for illustrating the phenomenon. As reported by [Saint-Marc et al. \(2008\)](#), this model considers the cement as an ageing material and it is based on the concept of cement degree of hydration  $\zeta$ , which is defined as the ratio of produced heat on total heat produced when all cement hydration is completed.

The macroscopic kinetic law of hydration that specifies the evolution of degree of hydration

is given by Arrhenius equation:

$$\frac{d\zeta}{dt} = A(\zeta)\exp(-E_a/R) \quad (5)$$

where  $(-E_a/R)$  is the Arrhenius constant, and  $A(\zeta)$  is the normalized affinity, which depends solely on the degree of hydration  $\zeta$  and the composition of the cement. It is evaluated on the basis of calorimetric tests.

$$C \frac{dT}{dt} + \text{div}(-K \text{grad}T) = A(\zeta)\exp(-E_a/R) \quad (6)$$

$\beta$  is a parameter that characterizes cement shrinkage/expansion. However, it cannot be applied, as it is, to cement sheath simulation because it implicitly assumes that cement sets at atmospheric pressure. This is why no pore pressure term appears in the equation.

$$d\bar{\sigma} = \frac{E(\zeta)}{1+\nu} d\bar{\varepsilon} + \frac{E(\zeta)}{3(1+2\nu)} \left( \frac{3\nu}{1+\nu} \text{tr}d\bar{\varepsilon} + 3\tau dT + 3\beta d\zeta \right) \bar{I} \quad (7)$$

There is not an existing model in the current literature to compute the state of effective stress under reservoir conditions in the cement sheath after cement has set.

### 3.10 Properties of hardened cement

Properties of solid cement can be subdivided into mechanical, hydraulic, and thermal.

1. Mechanical properties: characterize the response of cement to mechanical loads and deformations. These can further be subdivided into elastic properties and strength properties. The elastic properties are described by the Young's modulus and Poisson's ratio, while the strength properties are described by the unconfined compressive strength (UCS) and the tensile strength. When the stress in a compressive uniaxial test reaches a certain value, the specimen breaks down. The stress value at which this happens is the UCS. It describes the ability of cement to carry load under compression. However, it should be noted that cement set in the annulus is, in general, in a triaxial stress state. Triaxial tests can be used for a more detailed characterization of cement strength in compressive conditions. The Mohr-Coulomb criterion describes failure in compression. It needs to be supplemented with a tensile failure criterion to completely describe the strength of cement. This is usually done by specifying the tensile strength, i.e. the maximum magnitude of a tensile stress that the material can sustain without breaking apart. Compressive and tensile strength values are important characteristics of cement's load-bearing capacity. It should, however, be noted that annular cement can be subject to complicated stress paths and loading/unloading cycles during its lifetime. An important aspect of cement's mechanical behavior is that cement is a brittle material, i.e. it fails with very little preceding plastic deformation. Brittleness of cement is often estimated indirectly by means of its Young's modulus. Lower Young's modulus indicates a less brittle cement. Low Young's modulus improves the ability to deform without stresses becoming so high that they would exceed the strength of cement. Regrettably, lowering the Young's modulus by means of additives may degrade other properties of cement, in particular strength. See [Lavrov and Torsæter \(2016\)](#).

2. Hydraulic properties: hydraulic properties determine the ability to create a leak along the well or the rate which the cement sheath will be chemically degraded. If cement is properly placed, the leakage capacity is determined by cement's permeability. Permeability of currently used well cements is considered sufficiently low to prevent leakage if the cement remains intact.
3. Thermal properties: one of the mechanisms of fracture development in well cement is linked to heating and cooling. Thermal properties of cement play a crucial role, in particular the coefficient of thermal expansion in the contrast between casing, cement and formation with regard to it. Other thermal properties include the thermal conductivity and the specific heat capacity.

### 3.11 Initial stress state in annular cement sheath

According to [Saint-Marc et al. \(2008\)](#), initial stresses are the stresses that exist in cement sheath right after it has hardened. In theory, it might be possible to measure these stresses by installing pressure sensors in cement before it hardens, but this is not usually done. The initial stresses in cement depend not only on the properties of cement but also on the formation properties along the cemented section. Cement contraction may be facilitated by cement shrinkage caused by hydration. As a result of cement contraction, the cement column tends to move downwards, which creates shear stresses between cement and the walls exposed in the annulus. At the same time, the cement develops shear strength counteracting the downward movement of the cement column. The shear strength thereby reduces the hydrostatic pressure, as if the slurry were hanging on the walls exposed in the annulus. As a result, the vertical stress in the cement column at the bottomhole gradually decreases during setting. An additional reduction in the cement pressure can be due to the water loss from cement into the formation during cement setting. Reductions in hydrostatic pressure in cement slurry and in the pore pressure in set cement are amongst the factors usually held responsible for gas influx from formation into the annulus during well cementing, the phenomenon known as gas migration, see [Lavrov and Torsæter \(2016\)](#).

There seems to be no consensus in the industry about the magnitude of the initial stresses in cement. Different modelers base their simulations on different assumptions. For instance, [Gray et al. \(2009\)](#) assumed that cement is in a hydrostatic compressive state of stress after hardening (set the principal initial stresses equal to the hydrostatic pressure in the slurry column). A different approach is followed by [Bosma et al. \(1999\)](#), they considered three types of cement: shrinking, zero-shrinkage, and expanding. They argued that the initial stresses in a shrinking cement could be set equal to zero; the initial stresses in a zero-shrinkage cement could be set equal to the hydrostatic pressure of the slurry; and the initial stresses in expanding cement could be set to the hydrostatic pressure plus some expansion-induced extra stress.

As described above, assumptions about the initial stress values have significant consequences on the overall cement sheath integrity analysis. For example, tensile failure of cement is most relevant when the initial stresses in cement are low, zero or positive (traction). If these stresses are high and compressive, shear failure is likely to be the dominant failure mode when casing pressure or temperature are changed. See [Lavrov and Torsæter \(2016\)](#).

### 3.12 Effect of casing pressure increase and decrease on cement sheath

Casing pressure can increase during the following operations: well perforation, hydraulic fracturing, formation integrity test, casing pressure test, injection of fluids in oil and gas reser-

voirs. Expansion of the casing caused by the casing pressure increase tends to expand the surrounding cement and rock. As a result, the hoop stress in cement and rock will become less compressive, while the radial stress will become more compressive. Casing pressure can decrease during hydrocarbon production from the reservoir, when the bottomhole pressure drops from the initial pore pressure to the production pressure. When the casing contracts, the surrounding cement and rock will tend to move radially towards the well axis. As a result, the hoop stress in cement and rock will become more compressive, while the radial stress will become less compressive, see [Lavrov and Torsæter \(2016\)](#).

#### 4 NUMERICAL SIMULATION

In this section, a description of the modeling of the borehole cement sheath is presented. The stresses in the cement are calculated assuming that steel, cement, and the formation are thermoelastic materials. The model steps consider the variations of pressure, stress, and temperature that occur before and after the cement is set. The total strain tensor field is the superposition of elasticity deformation, plastic deformation, creep deformation, and thermal expansion:

$$\varepsilon_{ij} = \varepsilon_{ij}^e + \varepsilon_{ij}^p + \varepsilon_{ij}^{cr} - \varepsilon_{ij}^{th} \quad (i, j = 1, 2, 3) \quad (8)$$

The resulting differential equations system to be solved by the numerical technique of the Finite Element Method (FEM) is the equation that represents elasticity in a continuum medium without dynamic effects (9).

$$\overline{\nabla} \cdot \overline{\sigma} = -\overline{f} \quad (9)$$

where  $\overline{\nabla}$  is the divergence operator,  $\overline{\sigma}$  is the stress tensor, and  $\overline{f}$  is the external net force.

The borehole simulation plug-in introduced in this paper was developed by *Solaer* and runs under Abaqus 2016 platform.

##### 4.1 Cement mechanical behavior modeling

The cement model proposed for the numerical simulation is based on the variation of the elastic constants according to the degree of hydration. When the hydration process is beyond the gel point, the following parameters change:

- Young's modulus
- Shrinkage/Expansion
- Creep

The hydration degree law that we use does not come from a direct measurement. It is evaluated on the bases of calorimetric test taken from [Reddy et al. \(2007\)](#). Based on this work, we propose a law which meets the reported values.

1. Young's Modulus: the evolution of Young's modulus shows a close relationship to the evolution of the degree of hydration, so, the evolution of Young's modulus over time resembles the evolution of hydration.

We propose the following approximation (10) to model the Young's Modulus as a function of cure time, valid for the analyzed period (150 hs):

$$E(t) = E_f \frac{\log(t)}{\log(t_f)} \quad (10)$$

where  $E_f$  (Pa) is the hardened Young's modulus and  $t$  is the cure time in hs. Figure (8) shows the evolution of Young's module as a function of cure time up to its final value (hardened). In order to match the numerical values during the first 150 hs,  $t_f$  was set at 30,000 hs. Reddy's reported values are shown in red crosses.

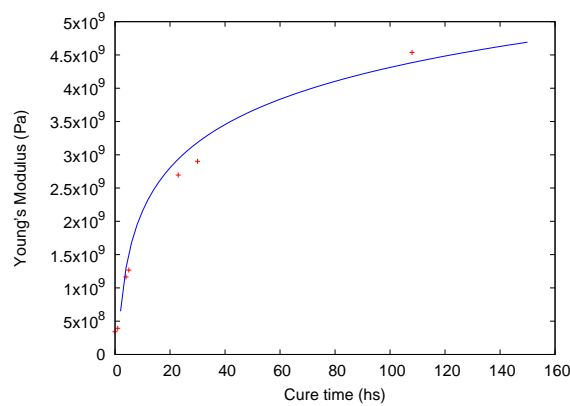


Figure 8: Young's Modulus as a function of cure time.

2. Shrinkage/Expansion: more than 95% of the contraction takes place during the first 50 hours of the hydration process. The shrinkage-induced reduction of cement bulk volume is in the range of 0.5 to 5%. See [Lavrov and Torsæter \(2016\)](#). Based on the experimental results of [Reddy et al. \(2007\)](#) work, a shrink-time relationship is shown according to the following equation(11):

$$V_s(t) = V_{sf} \frac{\log(t)}{\log(t_f)} \quad (11)$$

in the current model  $t_f$  was set at 50hs, and the final shrink value  $V_{sf}$  was set at -2.75%, as shown in figure (9).

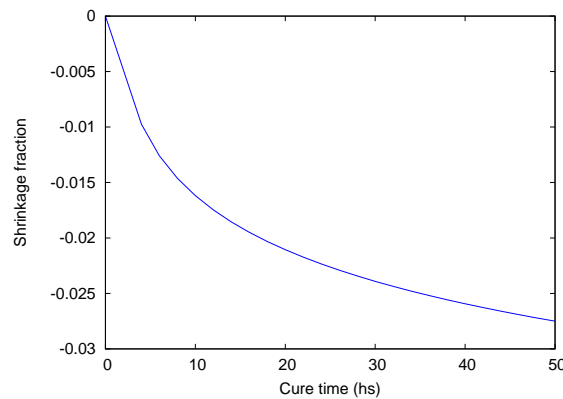


Figure 9: Shrinkage fraction vs Cure time (hs).

3. Creep: creep velocity is a function of the hydration degree and the stress state in every point as a function of time. No experimental data is available for different degrees of reaction, but the general behavior is that the strain rate is higher in tension than in compression and the strain rate is inversely proportional to the reaction degree, see [Saint-Marc et al. \(2008\)](#).

In order to show the importance of the creep effect on the initial stress field, the creep equation below is proposed:

$$\dot{\bar{\varepsilon}}(\zeta) = A(\zeta)\bar{q}^n t^m \quad (12)$$

where  $\bar{q}$  is the deviatoric stress tensor,  $n$  is the stress hardening power,  $m$  is the time hardening power, and  $A(\zeta)$  is the normalized affinity.

The coefficients were adjusted to obtain the following behaviors:

- (a) Creep Law 0 (CL0): inelastic deformation close to zero (no creep).
- (b) Creep Law 1 (CL1): inelastic deformation close to shrinkage (no stresses).
- (c) Creep Law 2 (CL2): inelastic deformation lower than contraction (residual stress is 0.1% of the tensile strength).

In order to reflect the influence of these three creep laws, figure (10) shows the case where the deviatoric stress is 2% of the maximum deviatoric stress as a function of the reaction degree.

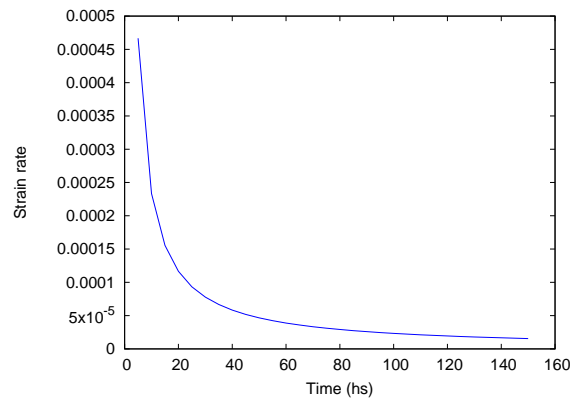


Figure 10: Strain rate vs time.

## 4.2 Borehole Geometry Design

For longer term zonal isolation is crucial to model the borehole geometry (eccentricity, deviation angle, casing diameter, cement sheath diameter, length, etc) see figure (11). If the borehole is not smooth, uniform, and in-gauge, it can have a significant effect on the result of the cementing operation. Improper centralization will adversely impact fluid velocity distribution around the pipe and casing and rheological hierarchy of mud, spacer, and cement fluids. Hence, borehole geometry, along with centralization, can significantly affect the stress uniformity around the cemented casing. See [Fjaer et al. \(2008\)](#); [Williams et al. \(2011\)](#).

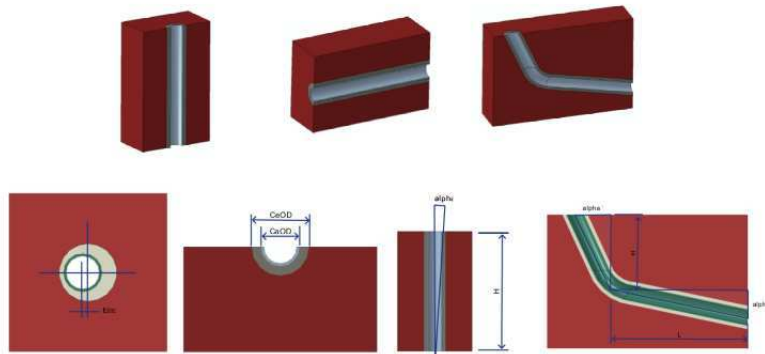


Figure 11: Solver Borehole Geometry input.

## 4.3 Materials

Formation inputs include formation elastic stiffness matrix  $C_{ijkl}$  for the general case or Young's modulus and Poisson's ratio for isotropic rocks, density, thermal conductivity, and expansion factor. Casing inputs include density, Young's modulus, Poisson's ratio, thermal conductivity, and thermal expansion factor. Cement inputs include density, compressive and tensile strengths, elastic stiffness matrix or Young's modulus and Poisson's ratio, expansion factor, and thermal conductivity. Figure (12) shows the solver input interface. An important parameter to consider when modeling mechanical properties of the cement to be used is the ratio

of cement-to-formation Young’s modulus. The lower the number, the more likely the cement is to remain intact in an elevated stress environment.

Cement Properties	Value	Unit	Formation Properties	Value	Units	Casing Steel Properties	Value	Unit
Material name	Manual input (name)	--	Formation name	Manual input (name)	--	Material name	Manual input (name)	--
Young's Modulus	Manual input (E)	Unit	Young's Modulus	Manual input (E)	Unit	Young's Modulus	Manual input (E)	Unit
Poisson's ratio	Manual input (nu)	Unit	Poisson's ratio	Manual input (nu)	Unit	Poisson's ratio	Manual input (nu)	Unit
Thermal Conductivity	Manual input (TC)	Unit	Thermal Conductivity	Manual input (TC)	Unit	Thermal Conductivity	Manual input (TC)	Unit
Density	Manual input (Rho)	Unit	Thermal Expansion	Manual input (TE)	Unit	Density	Manual input (Rho)	Unit
Tensile Strength	Manual input (St)	Unit				Tensile Strength	Manual input (St)	Unit
Compressive Strength	Manual input (Sc)	Unit				Compressive Strength	Manual input (Sc)	Unit
Thermal Expansion Coefficient	Manual input (alpha)	Unit				Thermal Expansion Coefficient	Manual input (alpha)	Unit

Figure 12: Solver Materials input.

#### 4.4 Loads

Stress Field and Pore Pressure:

Stress Field Component	Value	Unit
Stress Field name	Manual input (name)	--
Overburden	Manual input (sigma <sub>v</sub> )	Unit
Maximum horizontal	Manual input (sigma <sub>H</sub> )	Unit
Minimum horizontal	Manual input (sigma <sub>h</sub> )	Unit
Poral Pressure	Manual input (P <sub>0</sub> )	Unit

Figure 13: Solver Stress field and Pore pressure input.

Mud-Cement Pressure:

Mud/Cement Pressure	Value	Unit
Mud Pressure	Manual input (P <sub>m</sub> )	Unit
Cement Pressure	Manual input (P <sub>c</sub> )	Unit

Figure 14: Solver Mud-Cement pressure input.

Initial Temperature:

Initial Temperature	Value	Unit
Temperature	Manual input (T <sub>0</sub> )	Unit

Figure 15: Solver Initial Temperature input.

## 4.5 Life History

### Production:

Pressure decrease during production mainly affects the bottom of the hole. For example, an increase of the pressure on the external surface of the cement sheath represents a situation where the formation loads the wellbore. Far-field minimum stress changes can also occur following a change of reservoir pore pressure, see [Thiercelin et al. \(1998\)](#).

Poral Pressure	Value	Unit
Final Pore Pressure	Manual input ( Pf )	Unit ▼

Figure 16: Solver Final Pressure input.

### Fracture/Stimulation Treatment:

Stresses induced by stimulation may result in mechanical failure of the cement. Cement typically fails in tension, and failure occurs when the tangential stress is greater than the tensile strength of the cement sheath. Failure in tension can induce tensile cracking oriented vertically up the wellbore. These cracks may provide pathways for gaseous hydrocarbon fluids to migrate from the formation into water aquifers and/or to surface. It is important to reduce the Young's Modulus of the cement considerably below the Young's Modulus of the formation in order to mitigate the cracking. See [Thiercelin et al. \(1998\)](#); [Williams et al. \(2011\)](#).

Injection Pressure	Value	Unit
Injection Pressure	Manual input ( IP )	Unit ▼

Figure 17: Solver Injection Pressure input.

### Thermal Stimulation:

The type of failure, either cement debonding or cement cracking, is a function of the nature of the downhole condition variations. Thermo-elastic analysis allows to propose appropriate cement mechanical properties to avoid cement failure and debonding due to heat.

Final Temperature	Value	Unit
Temperature	Manual input ( Tf )	Unit ▼

Figure 18: Solver final temperature input

## 5 FIELD CASE MODEL

### 5.1 Geological Characteristics of the Study Area

The Neuquina Basin is located in the west-central Argentina covering an areal extension of 160,000 km<sup>2</sup>, see figure (19). As stated by Ramos (1998), its origin is linked to the history of the western margin of Gondwana, active since the Proterozoic. The basin is the most important Argentine basin in terms of hydrocarbon production and it is becoming a major site for unconventional reservoir development in South America.



Figure 19: Neuquina Basin Location.

The sedimentary sequence, which exceeds the 7000 m in thickness was deposited in a retroarc rift-related basin with subsidence controlled by thermal and compressional relaxation, see Howell et al. (2005); Cristallini et al. (2006). The basin stratigraphy is composed by several reservoirs, source rocks and seals as result of continental and marine sequences deposited from the late Triassic to early Cenozoic.

The analyzed production well is located in the Loma Jarillosa Este (LJE) block, which is placed in the embayment zone. A schematic stratigraphic column of LJE block is shown in figure (20).

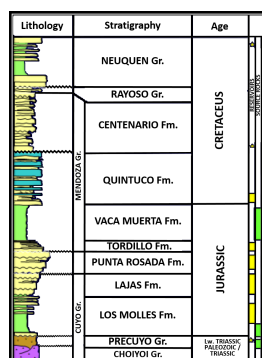


Figure 20: Stratigraphic column of LJE block.

According to Cristallini et al. (2006), the northeastern region of the basin, where LJE lies, is characterized by a Normal Stress field. Horizontal stresses direction go along with the local

tectonic regime. The maximum horizontal stress ( $\sigma_H$ ) azimuth varying from  $60^\circ$ - $240^\circ$  to  $90^\circ$ - $270^\circ$  (approximately in a west-east direction), see figure (21) taken from the World Stress Map.



Figure 21: WSM [Heidbach et al. \(2008\)](#)-Red perimeter closes the LJE block.

The production well is located in a highly stressed area approximately 500 meters far from a normal fault dipping with north-northeast orientation (fault damage zone). The cemented study interval is located in the Tordillo formation, which is one of the main reservoir of the basin. This formation is a clastic reservoir deposited through eolian and lacustrine mechanisms during late Jurassic, see [Vergani et al. \(1995\)](#). Table (1) shows the geomechanics properties of Tordillo formation estimated from the work published by [Osorio and Muzzio \(2013\)](#).

Formation	Tordillo
TVD	2440 m
$E_{stat}$	27.3 Gpa
$\nu_{stat}$	0.26522
$\rho$	2589.8 kg/m <sup>3</sup>
$T_{avarage}$	110°C
Thermal Conductivity	2.5 W/(m.k)
Thermal Expansion Coefficient	$1.25 \times 10^{-5}$ 1/°C
$\sigma_H$	54 Mpa
$\sigma_h$	50 Mpa
$\sigma_v$	74 Mpa
$P_p$	36 Mpa
Mud density	1200 kg/m <sup>3</sup>

Table 1: Tordillo's Isotropic Static Elastic and Thermal Properties-Field Stress and Poral Pressure.

The conventional borehole cement used for simulation is the class H. Its mechanical and thermal properties are listed in table (2). Also, mechanical and thermal properties of the casing are shown.

Material	Class H Cement	Casing (Steel)
$E$	1.4 Mpsi	29.732 Mpsi
$\nu$	0.15	0.3
$\rho$	16.4 lbm/gal	65.09 lbm/gal
Tensile Strength	465 psi	-
UCS	4350 psi	-
Thermal Conductivity	0.58 Btu/h.°F.ft	19 Btu/h.°F.ft
Thermal Expansion Coefficient	$5.1 \times 10^{-6} \text{ 1/°F}$	$1 \times 10^{-5} \text{ 1/°C}$

Table 2: Cement-Casing Elastic and Thermal Properties.

## 5.2 Borehole cement sheath integrity simulation

The analyzed vertical borehole section is located at a depth of 2440 m (TVD) with a centralized casing. The  $x$  axis of the reference frame is aligned with the maximum horizontal stress direction ( $\sigma_H$ ), and the  $y$  axis is aligned with the minimum horizontal stress direction ( $\sigma_h$ ). The cementing simulation steps are detailed below.

- Step 1: the model is initialized by looking for the reservoir geostatic equilibrium using the parameters listed in table (1) and (2).

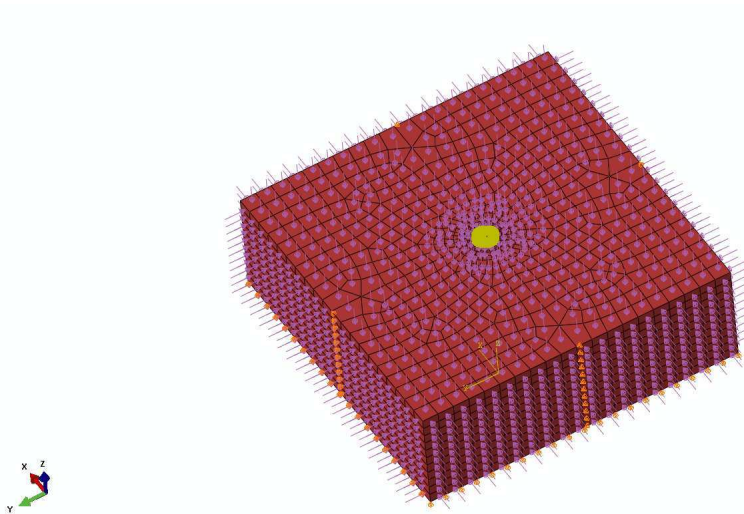


Figure 22: Reservoir geostatic equilibrium.

- Step 2: once the initial equilibrium has been reached, the borehole section is removed and the drilling mud pressure is applied to the formation wall.

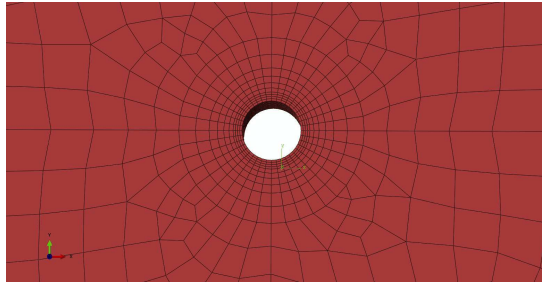


Figure 23: Drilling mud pressure applied to the formation wall.

- Step 3: the next step is the occurrence of casing, with internal and external pressures balanced with the mud pressure value.

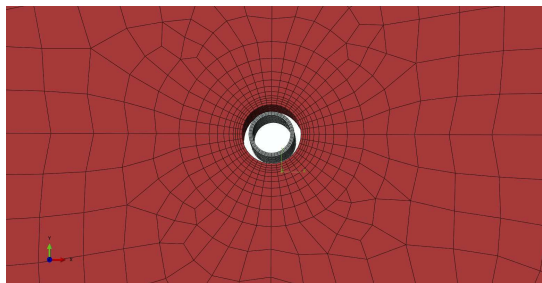


Figure 24: Casing placed.

The elements added in this step were previously created and set as disabled. Their activation is controlled by an Abaqus functionality called *Model Change*. In addition, this operation enables the contact interactions among the new elements and the preexisting ones.

- Step 4: this step incorporates the cement sheath as slurry. The pressure on the formation and the external casing surface are adjusted according to the cement hydrostatic pressure.

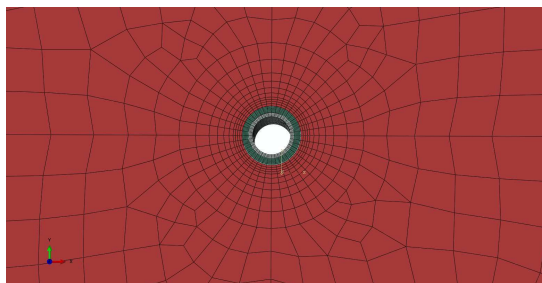


Figure 25: Cementing process.

The elements added in this step were previously created and set as disabled. Their activation is controlled by an Abaqus functionality called *Model Change*. In addition, this operation enables the contact interactions among the new elements and the preexisting ones.

- Step 5: the hardening process (from slurry to solid cement) is simulated by considering the following effects: set of hydrostatic pore pressure at zero (pressure between formation and external casing face), shrinkage, change of the elasticity modulus, creep, development of normal contact stresses, and cut-off against formation and casing.

Once the cement sheath is placed (with its resulting initial stress field), the model is ready to be tested for production and hydraulic stimulation.

## 6 RESULTS

In this section we show the results obtained for the field case simulation using creep laws CL0, CL1, and CL2.

### 6.1 Initial stress field after cement has set (150 hs)

- **CL0:** there is a correspondence between radial stress and minimum principal stress (figures (26) and (28)). For this combination of relative stiffness, all radial stresses are compressive. Comparing formation-cement interaction with casing-cement interaction, the difference in behavior is relevant. Radial stress is lower in the formation-cement interface, and in some cases (with a different relative stiffness or a higher shrinkage), an external microannulus can develop. Figures (27) and (29) show the correspondence between Hoop stress and Maximum principal stress. The tensile stress value reached is far over the allowable cement tensile strength. This highlights the importance of creep as a mechanism of stress relaxation; without its action, a set of cracks induced by Hoop stress will develop.

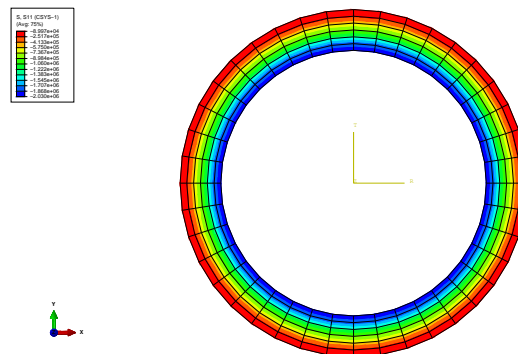


Figure 26: Radial stress on cement sheath (Pa).

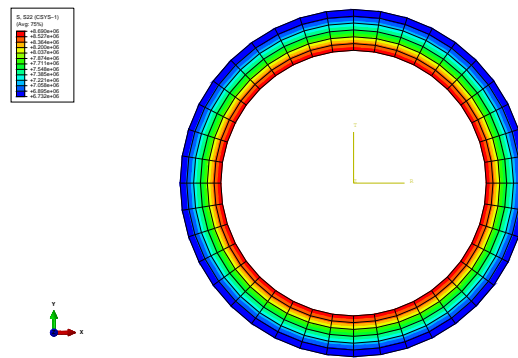


Figure 27: Hoop stress on cement sheath (Pa).

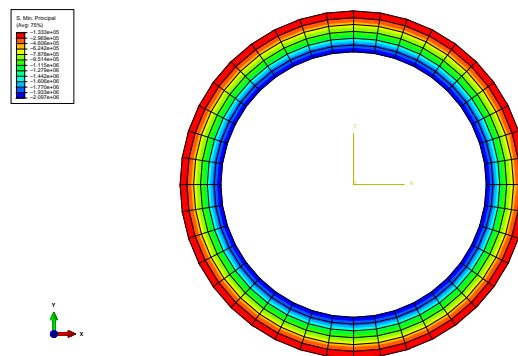


Figure 28: Minimum principal stress on cement sheath (Pa).

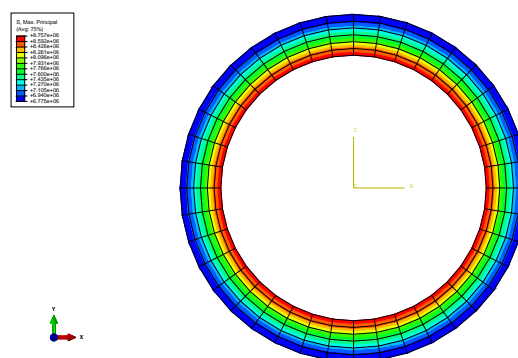


Figure 29: Maximum principal stress on cement sheath (Pa).

- **CL1:** figures (30) to (33) show the residual stress after the full set. Creep is relevant up to 150hs. Again, there is a correspondence between radial stress and minimum principal stress (figures (30) and (32)), and between Hoop stress and maximum principal stress (figures (31) and (33)). Comparing figures (28) and (32) the effect of creep over stress relaxation is evident. With CL1, tensile stresses are four orders of magnitude lower than

the previous results with CL0. The maximum principal stress reported is  $7.888 \times 10^2$  Pa, far from the allowable tensile stress ( $3 \times 10^6$  Pa).

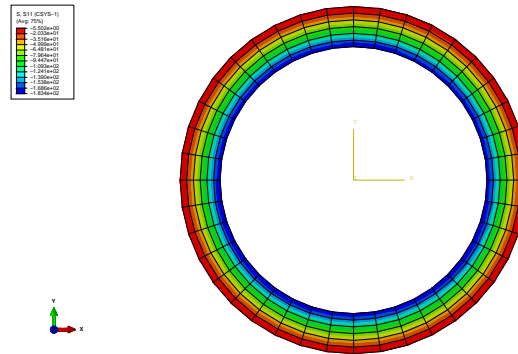


Figure 30: Radial stress on cement sheath (Pa).

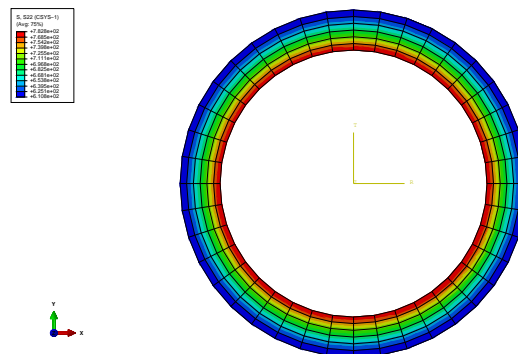


Figure 31: Hoop stress on cement sheath (Pa).

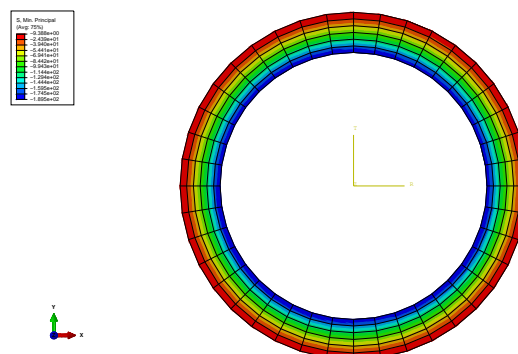


Figure 32: Minimum principal stress on cement sheath (Pa).

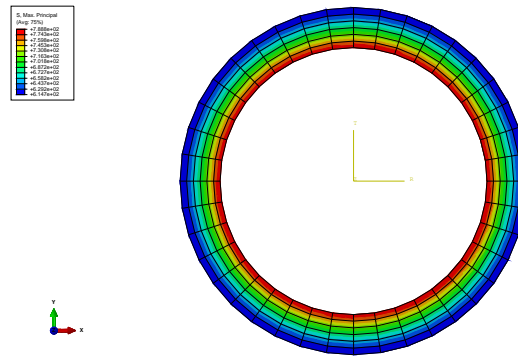


Figure 33: Maximum principal stress on cement sheath (Pa).

- CL2:** figures (34) to (37) show the residual stress after the full set. Creep is relevant up to 150hs. Again, there is a correspondence between radial stress and minimum principal stress (figures (34) and (36)), and between Hoop stress and maximum principal stress (figures (35) and (37)). Comparing figures (32) and (36) it is evident that the stress relaxation is lower in CL2. The maximum principal stress reported is  $1.16 \times 10^4$  Pa, still far from the allowable tensile stress ( $3 \times 10^6$  Pa), but two orders of magnitude higher than the results using CL1.

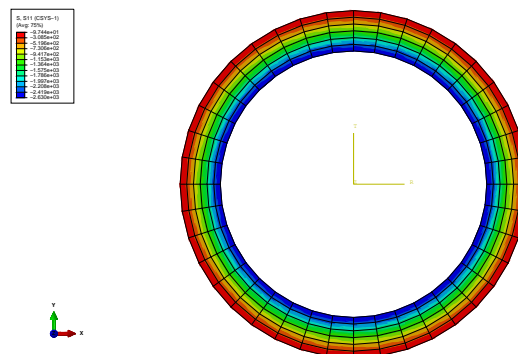


Figure 34: Radial stress on cement sheath (Pa).

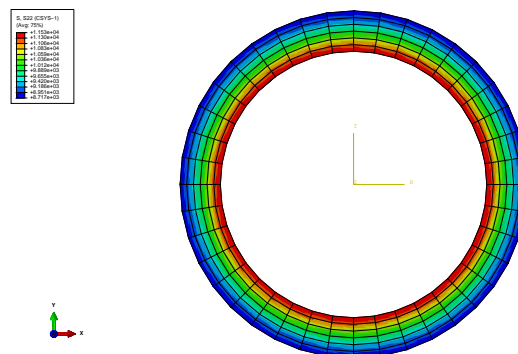


Figure 35: Hoop stress on cement sheath (Pa).

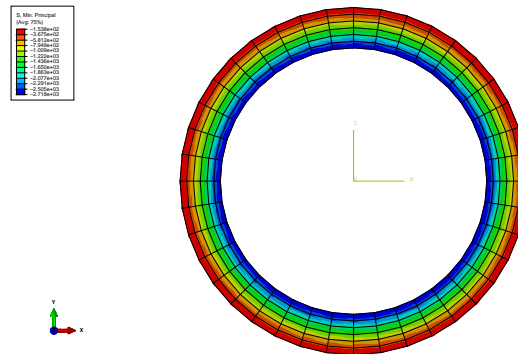


Figure 36: Minimum principal stress on cement sheath (Pa).

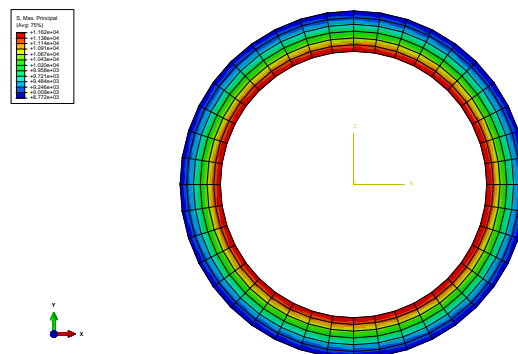


Figure 37: Maximum principal stress on cement sheath (Pa).

## 6.2 Hydraulic fracture stimulation and production

The hydraulic fracture pressure used in this test was  $4.826 \times 10^7$  Pa (7000 psi). Production was simulated as a drop of pore pressure to a half of the initial one. Consequently, all the effective stresses on the formation were incremented in  $1.44 \times 10^7$  Pa and the internal casing pressure was reduced in the same amount.

- **CL0:** not tested due to cement sheath crack developed during setting as shown in figure (27) (tensile stress over allowable limits).
- **CL1-Full cement set:** for this simulation, cement Young's modulus represents the long term material ( $E_f=9652720000$  Pa). Figures (38) and (40) show that the compressive stresses are radial and below the allowable limits. Figures (39) and (41) show that the Hoop stresses are high and in the order of the allowable tensile stress. The stress distribution across a radial path shows a different distribution than before (regardless of the numerical values). This is due to a plastic flow in the interface between casing and cement sheath. It is confirmed by figure (42). Here the equivalent plastic strain is not zero, this means that the yield surface was reached. In a quasi-brittle material, it represents a radial crack induced by Hoop stress. Production was not tested because at this point the cement sheath has already failed.

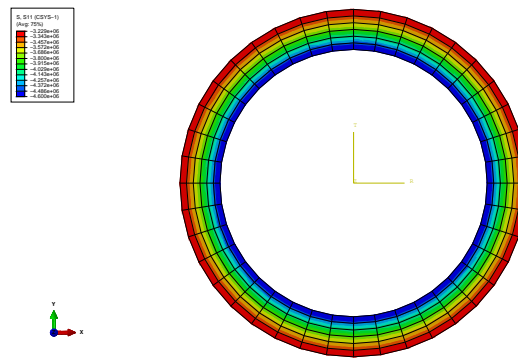


Figure 38: Radial stress on cement sheath (Pa).

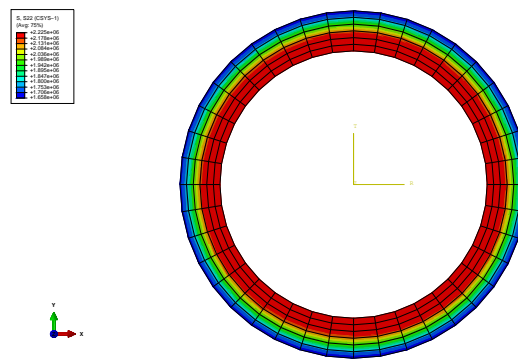


Figure 39: Hoop stress on cement sheath (Pa).

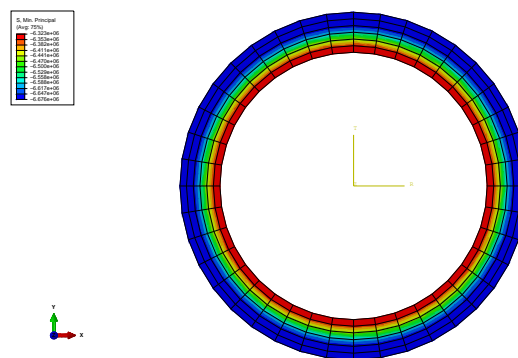


Figure 40: Minimum principal stress on cement sheath (Pa).

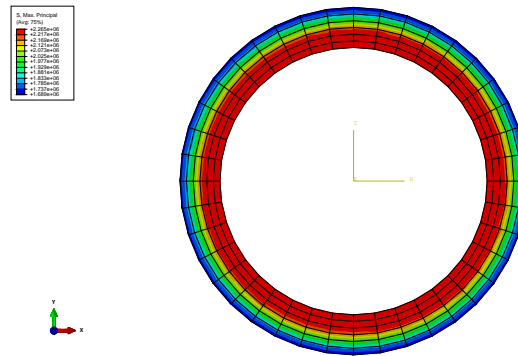


Figure 41: Maximum principal stress on cement sheath (Pa).

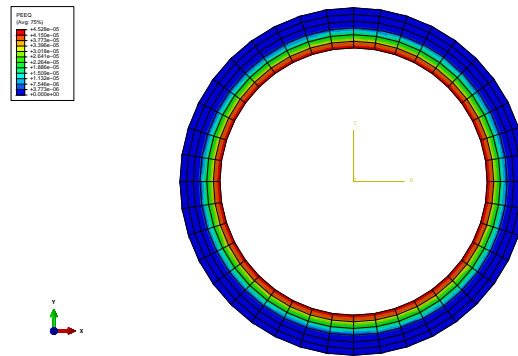


Figure 42: Equivalent plastic strain.

- CL1-50hs after cement set:** In some cases, the hydraulic fracture stimulation can be performed a short time period after the cement sheath has set. For this test, cement properties and initial stresses were applied 50hs after cement set according to Reddy's work. Young's modulus of  $3 \times 10^9$  Pa was used. A strength of 70% of full set strength is expected. Figures (43) and (45) show that the compressive stresses are radial and below the allowable limits. Figures (44) and (46) show that the tensile stresses are lower than the previous case. The stress distribution across a radial path shows a similar distribution before and after the hydraulic fracture stimulation. Figure (47) confirms that the yield surface was not reached.

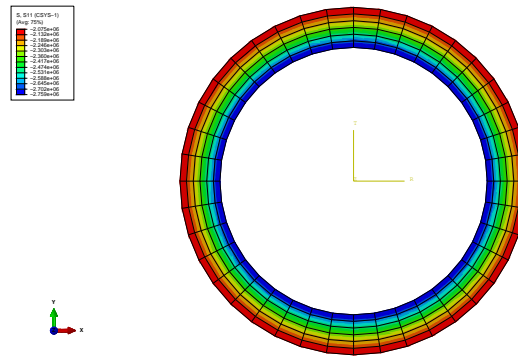


Figure 43: Radial stress on cement sheath (Pa).

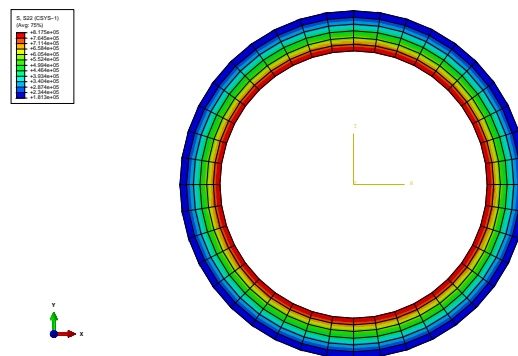


Figure 44: Hoop stress on cement sheath (Pa).

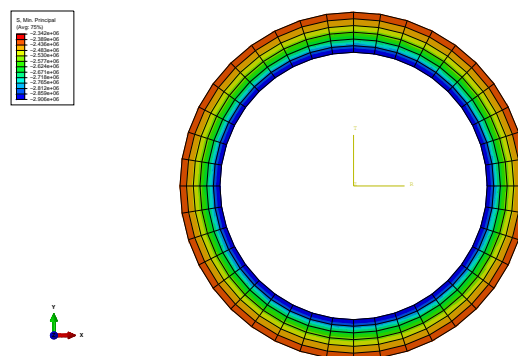


Figure 45: Minimum principal stress on cement sheath (Pa).

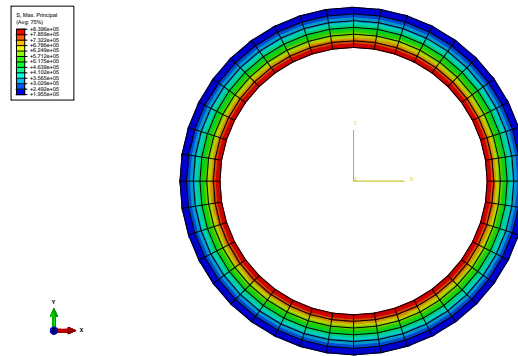


Figure 46: Maximum principal stress on cement sheath (Pa).

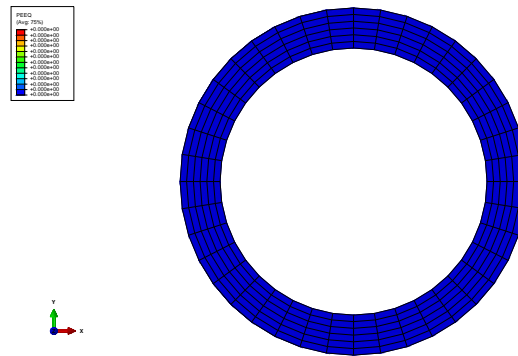


Figure 47: Equivalent plastic strain.

When the production takes place, the effect evaluated is a long term effect. Because of that, the full set parameters were used. Figures (48) to (51) show that all stresses are compressive. This behavior is justified because the reduction in pore pressure produces an increment in the effective stress; the horizontal stresses try to close the borehole. The stress values are in the allowable range. It is confirmed by figure (52) (zero PEEQ).

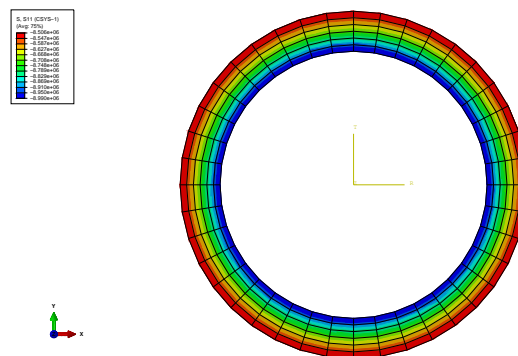


Figure 48: Radial stress on cement sheath (Pa).

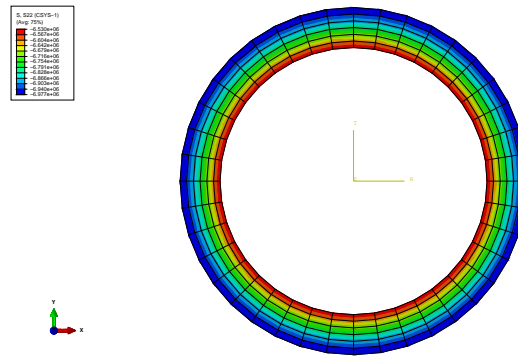


Figure 49: Hoop stress on cement sheath (Pa).

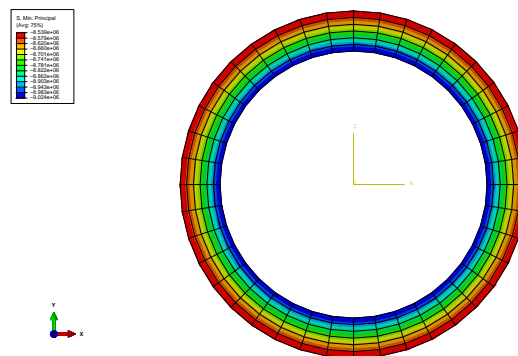


Figure 50: Minimum principal stress on cement sheath (Pa).

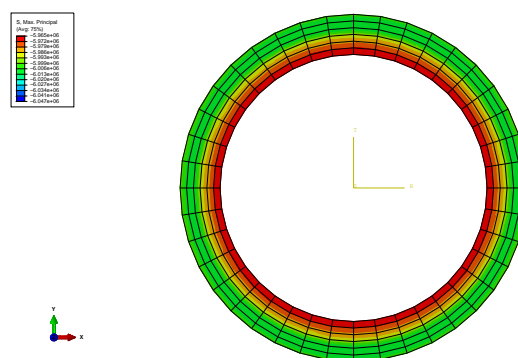


Figure 51: Maximum principal stress on cement sheath (Pa).

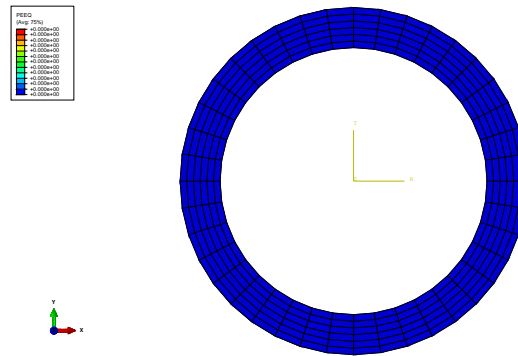


Figure 52: Equivalent plastic strain.

- CL2-50hs after cement set:** figures (53) and (54) show maximum and minimum principal stresses. Values seems to be within the allowable range, but the yield criteria is triaxial and figure (55) shows that PEEQ is not zero. It means that the yield surface was reached. Again, It represents a crack in a quasi-brittle material. The result shows that a little initial stress can affect cement sheath behavior adversely. Note that CL2 was tuned in order to have this result.

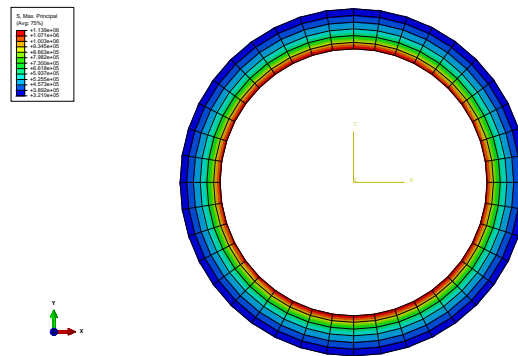


Figure 53: Maximum principal stress on cement sheath (Pa).

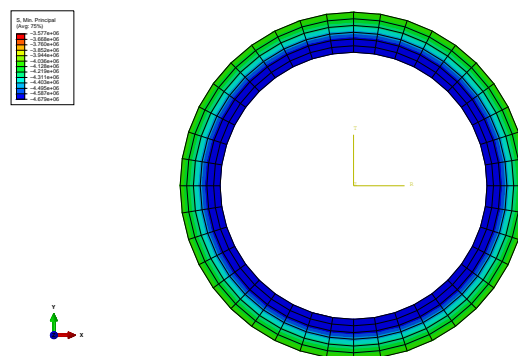


Figure 54: Minimum principal stress on cement sheath (Pa).

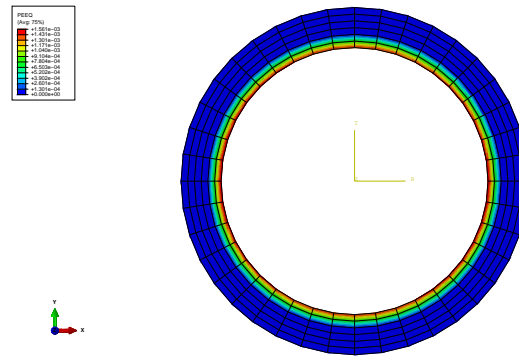


Figure 55: Equivalent plastic strain.

## 7 CONCLUSIONS

Creep is the main stress relaxation mechanism that appears on the cement sheath during the setting process. These stresses are generated by reduction of the pore pressure, appearance of shear stresses on the cement-formation and cement-casing interfaces, shrinkage, and swelling related to thermo-chemical effects. The initial state of stress after cement setting is strongly dependent on the strain rate during the hydration process and the setting time. Small variations in the initial state of stress can mean the difference between a proper zonal isolation or a faulty one. Radial compressive stresses after cement setting depend not only on the creep law and the volumetric changes, but also on the relationships between the Young's modulus of the cement-formation and cement-casing interfaces. This ratio between modules is also important during the hydraulic fracture stimulation. In this process, tensile Hoop stresses are developed, which can give place to radial tensile faults. In the case that the fracture stimulation be performed a few hours after cement setting, the Young's modulus is lower, which means the stiffness ratio between cement and formation is more favorable. Additionally, when a displacement of the casing occurs, the developed stresses are smaller. The effect of pore pressure reduction in the formation due to production mainly generates compressive stresses. This effect is relevant in cements that suffer expansion during set. In these cases, the initial stress field is compressive. In the tested field case, the production is far from generating penetration of the yield surface. The plug-in developed by Solaer allows to test different cement formulations under reservoir conditions in a short time, following an easy workflow. This way, the cement engineer holds a powerful tool to choose the best combination of cement and operational practice for a specific well.

## REFERENCES

- Backe K., Lile O., Lyomov S., Elvebakk H., and Skalle P. Characterizing curing-cement slurries by permeability, tensile strength, and shrinkage. *SPE paper 38267- Western Regional Meeting*, 1997.
- Bosma M., Ravi K., van Driel W., and Schreppers G. Design approach to sealant selection for the life of the well. *SPE paper 56536- Annual Technical Conference and Exhibition*, 1999.
- Cristallini E., Bottesi G., Gavarrino A., Rodriguez L., Tomezzoli R., and Comeron R. Synrift geometry of the neuquén basin in the northeastern neuquén province, argentina. *Geological Society of America Special Paper 407*, 2006.

- Fjaer E., Holt R., Horsrud P., Raaen A., and Risnes R. *Petroleum Related Rock Mechanics*, volume 53. Elsevier, 2nd ed., 2008.
- Gray K., Podnos B., and Becker E. Finite-element studies of near-wellbore region during cementing operations. *SPE Drilling and Completion*, 24(1):127–136, 2009.
- Heidbach O., Tingay M., Barth A., Reinecker J., Kurfieb D., and Muller B. The world stress map database release 2008. *doi:10.1594/GFZ.WSM.Rel2008*, 2008.
- Hofmann B. and Moritz H. *Physical Geodesy*. Springer, 2005.
- Howell J., Schwarz E., Spalletti L., and Veiga G. *The Neuquén Basin: an overview. In The Neuquén Basin, Argentina: A Case Study in Sequence Stratigraphy and Basin Dynamics*. Geological Society, London, Special Publications, 252., 2005.
- Lavrov A. and Torsæter M. *Physics and Mechanics of Primary Well Cementing*. Springer, 2016.
- Nelson E. and Guillot D. *Well Cementing-Vol II*. Schlumberger, 2006.
- Osorio J. and Muzzio M. Correlation between microseismicity and geomechanics factors affecting the hydraulic fracturing performance in unconventional reservoirs-a field case in the neuquén basin, argentina. *ARMA 12-221.Mechanics/Geomechanics Symposium.*, 2013.
- Ramos V. Tectonic of the late proterozoic-early paleozoic: a colisional history of southern south america. *Episodes 11(3): 168-174*, 1998.
- Reddy B., Xu Y., Dennis Gray W., and Pattillo P. Cement shrinkage measurement in oilwell cementing-a comparative study of laboratory methods and procedures. *SPE paper 103610*, 2007.
- Saint-Marc J., Garnier A., and Bois A. Initial state of stress:the key to achieving long-term cement-sheath integrity. *SPE paper 116651-Annual Technical Conference held in Denver, Colorado, USA*, 2008.
- Thiercelin M., Dargaud B., Baret J., and Rodriguez W. Cement design based on cement mechanical response. *SPE-Drilling and Completion*, 13(4):266–273, 1998.
- Vergani G., Tankard A.J.and Belotti H., and Welsink H. Tectonic evolution and paleogeography of the neuquén basin, argentina.in aapg memoir 62: Petroleum basins of south america. *The American Association of Petroleum Geologists*, 1995.
- Williams H., Khatri D., Keese R., Le R., Roye J., Leach D., Rodriguez J., Rottler P., and Porcherie O. Flexible, expanding cement system (fecs) successfully provides zonal isolation across marcellus shale gas trends. *SPE 149440*, 2011.
- Zoback M. *Reservoir Geomechanics*. Cambridge University Press, 2007.